HAL
open science

In situ gas monitoring by fiber-coupled Raman spectrometry for H_2-risk management in nuclear containment during a severe nuclear aAccident

Sylvain Magne, Simon Nehr, Xavier Buet, Ahmed Bentaïb, Emmanuel Porcheron, Romain Grosseuvres, Etienne Studer, Roberta Scarpa, Daniele Abdo, Jean-Luc Widloecher, et al.

To cite this version:

Sylvain Magne, Simon Nehr, Xavier Buet, Ahmed Bentaïb, Emmanuel Porcheron, et al.. *In situ* gas monitoring by fiber-coupled Raman spectrometry for H_2-risk management in nuclear containment during a severe nuclear aAccident. IEEE Transactions on Nuclear Science, 2020, 67 (4), pp.617-624. 10.1109/TNS.2020.2965622 . cea-04385873

HAL Id: cea-04385873

https://cea.hal.science/cea-04385873v1

Submitted on 11 Jan 2024

HAL is a multi-disciplinary open access archive for the deposit and dissemination of scientific research documents, whether they are published or not. The documents may come from teaching and research institutions in France or abroad, or from public or private research centers.

L'archive ouverte pluridisciplinaire **HAL**, est destinée au dépôt et à la diffusion de documents scientifiques de niveau recherche, publiés ou non, émanant des établissements d'enseignement et de recherche français ou étrangers, des laboratoires publics ou privés.

In situ gas monitoring by fiber-coupled Raman spectrometry for H_2-risk management in nuclear containment during a severe nuclear accident

Sylvain Magne, Simon Nehr, Xavier Buet, Ahmed Bentaïb, Emmanuel Porcheron, Romain Grosseuvres, Etienne Studer, Roberta Scarpa, Daniele Abdo, Jean-Luc Widloecher, Olivier Norvez, Nabiha Chaumeix, Julien Dhote, Mathilde Freyssinier and Audrey Ruffien-Ciszak

***Abstract*—During a severe nuclear accident leading up to core melting, Molten Corium-Concrete Interaction (MCCI) and core-coolant water reaction both release large amounts of hydrogen (H_2) gas in the containment atmosphere. According to the Shapiro ternary diagram and depending on local partial pressures of H_2, air and water vapor, deflagration/detonation may occur with potential deleterious impact over equipment and structures. CO and CO_2 are also of interest, as revealing gases for MCCI. Pressurized Water Reactors (PWR) of French Nuclear Power Plants (NPPs) are equipped with Passive Autocatalytic Recombiners (PARs), partly mitigating the H_2-risk. However, the H_2-risk management strategy may be significantly improved by performing *in-situ* monitoring of H_2, O_2, N_2, H_2O, CO and CO_2 partial pressures at several locations inside the containment, to account for potential local combustion risk. Raman spectrometry involves only one laser and spectrometer equipped with a 2D Charge-Coupled Device (CDD). Raman probes are chemically selective and may be radiation-hardened. Custom-made fiber-coupled Raman probes, linked with a readout unit, were qualified in a climatic chamber, a flame-propagation tube, a ^{60}Co irradiation cell, a 3D shaking table, a steam jet and the MISTRA facility (1/10 reduced-scale containment mock-up dedicated to thermo-hydraulic tests).**

***Index Terms*—Hydrogen, Nuclear Power Plant (NPP), Severe Accident (SA), Raman Spectrometry.**

This work was done within the MITHYGENE Project, managed by the French *Agence Nationale de la Recherche* (ANR). This project was funded by the *Programme Investissements d'Avenir* (PIA), *Recherche en Sureté Nucléaire et Radioprotection* (RSNR) and co-funded by Air Liquide and EDF.

S. Magne, S. Nehr and X. Buet are with CEA, LIST, Laboratoire Capteurs Fibres Optiques, F-91191 Gif-sur-Yvette, France (sylvain.magne@cea.fr).

A. Bentaïb and R. Grosseuvres are with IRSN, PSN-RES/SAG, BP17, F-92262 Fontenay-aux-roses, France (ahmed.bentaib@irsn.fr).

E. Porcheron is with IRSN, PSN-RES/SCA, BP68, F-91192 Gif-sur-Yvette, France (emmanuel.porcheron@irsn.fr).

E. Studer, R. Scarpa, D. Abdo, J-L. Widloecher, O. Norvez are with CEA/DEN, DANS/DM2S/SFME/LTMF, CEA/SACLAY, F-91191 Gif-sur-Yvette, France (etienne.studer@cea.fr).

N. Chaumeix is with CNRS/Institut ICARE, 1C route de la Recherche scientifique, F-45071 Orléans, France (chaumeix@cnrs-orleans.fr).

J. Dhote, A. Ruffien-Ciszak, M. Freyssinier are with ARCYS, 14 place Marcel Dassault, BP70048, F-31702 Blagnac Cedex, France (julien.dhote@arcys.fr).

During a severe nuclear accident leading up to core melting, the reaction of core constituents with coolant water releases large amounts of hydrogen (H_2) gas in the containment atmosphere of Nuclear Power Plants (NPP). At an advanced stage of the accident, Molten Corium-Concrete Interaction (MCCI) releases hydrogen as well and carbon monoxide (CO), another flammable gas [1].

Depending on local partial pressures of H_2, air and water vapor (plotted on the Shapiro-Moffette ternary diagram [2]), deflagration or detonation may occur with potential deleterious impact over equipment and structures. The measurement of partial pressures of H_2, O_2, N_2 and H_2O in several locations inside the containment is therefore required to assess for the H_2-risk. Furthermore, the monitoring of additional gases such as CO and CO_2 provides complementary information about MCCI.

Large release of hydrogen gas within a nuclear containment happened several times in the past. In Three-Mile Island (USA) in 1979, a loss-of-coolant accident (LOCA) released about 460 kg of H_2 although the containment integrity was preserved. This severe accident (SA) was later rated as INES 6/7 (International Nuclear and radiological Event Scale). More recently, the nuclear accident that occurred in Fukushima-Daïchi (Japan) in March 2011, in the wake of a massive tsunami, is the worst since Chernobyl (INES 7/7) [3]. Several H_2 explosions had spread radionuclides in the atmosphere, prompting Japanese authorities to order population evacuation within a 30-km radius area around the site.

I. State-of-the art of H_2-risk mitigation strategies

To circumvent this H_2-risk, Pressurized Water Reactors (PWRs) may be equipped with Passive Autocatalytic Recombiners (PARs). The released hydrogen recombines with the oxygen present in the containment atmosphere. However, PARs only provides partial mitigation because the rate of H_2 generation at early times of the accident may exceed the H_2-recombination rate. Furthermore, in France, two PARs are actually equipped with thermocouples to detect presence of H_2 within each containment building, taking profit of the exothermic O_2-H_2 reaction. Nevertheless, the measured temperature does not provide sufficient information to assess

for the H_2-risk yet.

As an optional device dedicated to the European Pressurized Reactor (EPR), the Hermetis system (High Superheated Micro Sample Transport and Gas Analysis) has been qualified for SA conditions by the Framatome Co. (formerly AREVA NP) [4]. This system uses super-heated sampling pipes for transporting gases out from the containment into a recirculation module where they are analyzed and eventually sent back into the containment. Framatome announces selective measurements of H_2 and H_2O with capability to detect CO and O_2.

However, according to the French safety doctrine, sampling pipes are precluded in order to maintain containment tightness. Furthermore, the sampling operation itself conveys many other difficulties.

First, pipes are intended to be deployed within the containment building and to go through the concrete wall. A total length of at least 10 to 20 meters is necessary for that purpose. Therefore, the transit time of gases through the pipe imposes a significant delay time between gas sampling and measurement, in contradiction with the need to react quickly and to provide reliable data to safety authorities at early times of the accident (*i.e.* within the first ten minutes).

Second, although the pipes are heated (as a means to reduce adsorption), part of the gas is adsorbed along the internal surface of the pipe, thus altering the mixture proportion at the output. In that sense, water vapor is particularly problematic because, as a polar molecule, H_2O strongly adheres on many surfaces. Consequently, estimations of partial pressures are likely to be biased, especially H_2O *vs* H_2, O_2 and N_2, particularly at early times of the accident where equilibrium is not yet achieved between the gas-phase and the adsorbed one.

Third, the sampling operation extracts a large volume of gas which smoothes out local concentration gradients, thus leading to an underestimation of local detonation risks.

For all these reasons, an *in situ* monitoring of pressures in the gas phase is a prerequisite for guaranteeing accurate measurements inside the containment volume. Finally, a resident sampling/analysis system relies on a local power supply which may go down, as has happened in Fukushima.

The H_2-risk management strategy may be significantly improved by monitoring all gases of interest at several locations inside the containment in order to account for inhomogeneity and potential local detonation risk. The plant operator may then trigger H_2-risk mitigation techniques such as nitrogen shrouding or water spraying, according to the Severe Accident Management Guideline (SAMG).

A readout unit may be placed away from the radiological perimeter, fiber-connected to the passive probes located inside the containment and potentially powered by emergency power supplies in case of power outage. SA-qualified optical penetrations are commercially available and may be implemented in substitution to existing electrical ones. However, the number of penetrations available in nuclear containments is restricted (leakage criterion). This in turn restricts the number of fibers that may be interconnected.

II. OVERVIEW OF GAS MONITORING TECHNOLOGIES SUITABLE TO H_2-RISK ASSESSMENT

A. *H_2 measurement solutions*

Hydrogen is usually monitored using fuel cells, conductance (Pt/Pd, SnO_2), catalytic or palladium (Pd)-based sensors and Schottky diodes/MOSFET transistors [5]. Fuel cells rely on the measurement of an electric current proportional to the concentration of H_2 gas passing through a permeable layer, granted that the oxygen concentration is known. Conductance sensors exhibit a variation of electrical resistivity with respect to H_2 concentration. Catalytic sensors ("pellistors") rely on the change in temperature with the concentration of H_2 reacting in air on a hot wire. Finally, Pd-based sensors are based on the property of the palladium material to absorb large quantities of H_2 gas and to experience large volume or resistivity changes.

All these sensors are more or less sensitive to poisoning (*e.g.* by CO or combustion products) and may exhibit cross-sensitivity with other gases. Despite these limitations, several sensors are already qualified for SA monitoring, as Pd-based or catalytic sensors. As explained before, the use of a H_2 sensor alone does not provide an accurate assessment of the H_2-risk, although it yet provides the required redundancy in the context of nuclear safety. Since the concentrations of other gases cannot be considered as stable during an accident (O_2 is partly used up by PARs and, depending on nuclear reactor technology, H_2O or N_2 may be injected into the containment for mitigation purpose), complementary sensors dedicated to N_2, O_2 and H_2O are then necessary to provide an H_2-risk assessment. Besides, CO and CO_2 (MCCI tracers) should be monitored as well. Besides obvious cost and maintenance considerations, putting together several gas monitoring technologies that have nothing in common raises an issue about self-consistency of the collected data and their time evolution during NPP's lifespan, considering the impossibility to get access to the devices for recalibration purpose.

In the following, we show that *in situ* optical-based multi-gas sensing solutions provide a smart alternative to this situation. Furthermore, optical-based solutions lend themselves to the use of optical fibers linking probes to the instrumentation placed away from the radiological perimeter.

B. *Alternative multi-gas optical-based techniques*

Optical-based techniques mainly involve absorption or Raman scattering spectrometry techniques. Let us consider the visible or the near infrared (NIR) range of the optical spectrum, suitable for light transmission through optical fibers. In this optical range, the absorption technique is not well suited to symmetric molecules such as N_2 and H_2 because useful optical transitions are dipolar-electric forbidden [6]. Long interaction lengths are thus necessary to compensate for lesser efficiency, in contradiction with the requirement for a localized measurement. Finally, infrared (IR) laser diodes are often used to perform absorption spectrometry at the expense of flexibility, as the wavelengths are set to absorption bands of expected species. It is worthwhile noticing that none of these

techniques can detect noble gases (Xe, Ar, etc.).

Unlike the absorption technique, all molecules of interest (H_2, O_2, N_2, H_2O, CO, CO_2) exhibit efficient Raman signatures [7]. Spontaneous Raman Scattering conveys many other decisive advantages: simplicity, flexibility, chemical-selectivity, distributed and local gas detection (~ mm^3). Raman gas probes are compact, robust (passive optics, no electronics), and may be radiation-hardened.

III. In situ gas monitoring using fiber-coupled Raman spectrometry

A. Raman Spectrometry (RS) basics

RS has proven a versatile tool for molecular identification. It relies on the observation of inelastically scattered light and allows for studying vibrational and rotational modes of molecules. Mostly available for the analysis of liquid and solids, this technique is adaptable to the gas phase despite the lower density. RS was applied successfully to characterize inactive thermo-hydraulic conditions representative of a severe accident (air, steam mixture and aerosol at pressure and temperature) using a prototype probe [7]. One of the main difficulty of this technique is to separate the useful Stokes Raman light from the residual (Rayleigh scattered) laser light. In this study, all species of interest are light molecules of large Raman Stokes shifts, ranging typically from 1285 cm^{-1} (CO_2) up to 4164 cm^{-1} (H_2) making discrimination easier with conventional high-pass filters.

The Raman/laser ratio is very weak in single-pass configuration: of the order of ~ 10^{-15} (*i.e.* 1 fW for a laser power of 1 W). Therefore, Raman experiments often involve photon-counting detectors yielding, after integration, Raman signals S (in counts) proportional to photon flux n_{Raman} (ph/s). Acquisition times are typically of several minutes.

The Raman photon flux per unit solid angle (ph/sr) and per molecule depends on laser flux (ph/s.cm^2) as follows:

$$n_{Raman}(ph/sr.s) = \left(\frac{d\sigma}{d\Omega}\right) \cdot n_{laser}\ (ph/cm^2.s) \qquad (1)$$

where $\left(\frac{d\sigma}{d\Omega}\right)$ is the Raman differential cross-section [8-11], typically of the order of 10^{-31} cm^2/sr (1.45 10^{-31} cm^2/sr for the vibronic mode of nitrogen (N_2) at the wavelength of 640 nm).

The amount of collected light critically depends on light collection efficiency, according to the equation:

$$n_{Raman}(ph/s) = K \cdot I_{Laser} \cdot \left(\frac{d\sigma}{d\Omega}\right) \cdot \Delta\Omega \cdot \mathrm{N} \qquad (2)$$

where I_{laser} is the beam intensity (W/cm^2), N is the number of molecules in the observed volume V, $\Delta\Omega$ (sr) is the solid angle for light collection and K is an unitless experimental factor (accounting for quantum efficiency of the detector, grating diffraction efficiency, etc.).

As N = n N_A, where n is the molar concentration (in mole) and N_A is the Avogadro number (6.023 10^{23} molecules/mole), Eq (2) becomes:

$$S = K' \cdot I_{Laser} \cdot \left(\frac{d\sigma}{d\Omega}\right) \cdot \Delta\Omega \cdot \mathrm{n} \cdot \mathrm{t} \qquad (3)$$

where t is the integration time (in seconds). Assuming ideal gas behavior, one may write:

$$P = R \cdot T \cdot \mathrm{n/V} \qquad (4)$$

where R is the gas constant (8.314 $J.mol^{-1}.K^{-1}$), T is the temperature (in K) and P is the partial pressure (in Pa) in the gas phase. Substituting for n into Eq (3), we get:

$$S \cdot T = K' \cdot I_{Laser} \cdot \left(\frac{d\sigma}{d\Omega}\right) \cdot \Delta\Omega \cdot \frac{\mathrm{V}}{\mathrm{R}} \cdot \mathrm{P} \cdot \mathrm{t} \qquad (5)$$

Eq (5) shows that the partial pressure is a linear function of the Raman signal multiplied by the temperature T.

The laser power (in W) is related to laser intensity (in W.cm^{-2}) by the relation $P_{laser} = I_{laser}\ \pi.\omega^2$, where ω is the laser waist. In transverse observation, when ω is smaller than the core radius a, then V ~ 2a ($\pi\omega^2$), where a is the core radius of the collecting fiber. Then, Eq (5) reduces to:

$$S \cdot T = K' \cdot P_{Laser} \cdot \left(\frac{d\sigma}{d\Omega}\right) \cdot \Delta\Omega \cdot \frac{\mathrm{P}}{\mathrm{R}} \cdot (2\mathrm{a}) \cdot \mathrm{t} \qquad (6)$$

Furthermore, the solid angle for light collection depends on the half-angle of collection β according to:

$$\Delta\Omega = 2\pi \cdot (1 - cos\beta) \qquad (7)$$

that itself depends on the numerical aperture of the fiber NA = sin β. There always exists an optimal distance for which the collected light is maximum [12], related to the NA of the fiber, *i.e.* in our case: NA = 0.22, β = 12°, $\Delta\Omega = 0.15$ sr. This optimal distance is ~ 4.5 times the core radius and the Raman light only depends on core size and acceptance angle (Eq (6)).

Table I shows the Raman shifts of vibronic modes of H_2, H_2O, N_2, CO, O_2 and CO_2 along with their cross-sections relative to that of N_2, usually considered a reference gas, granted its inertness. Finally, the expected Raman wavelengths are also given for a laser wavelength of 640 nm.

Chemical selectivity is achieved with this technique if the Full Width at Half Maximum (FWHM) of a single Raman peak is less than the smallest wavelength difference (SWD) between adjoining Raman peaks (Rayleigh criterion). In our case, the SWD is 168 cm^{-1} (shift between O_2 and CO_2). Practically, a FWHM of less than 8 nm is required to

TABLE I
VIBRONIC RAMAN SHIFTS FOR MOLECULES OF INTEREST IN THIS STUDY

Molecule	ΔE (cm^{-1})	$\left(\frac{d\sigma}{d\Omega}\right) / \left(\frac{d\sigma}{d\Omega}\right)_{N2}$	Raman shift (nm) (*vs* laser @640 nm)
H_2	4161	2.4	872
H_2O	3652	3.2	835
N_2	2331	1	752
CO	2145	1	742
O_2	1556	1.2	711
CO_2	1388	1.3	704
	1285		697

Data from [9]-[10]-[11]

distinguish all the expected species, with the current setup.

In practice, a background (BG) spectrum is recorded at zero laser power. Then, Raman spectra are recorded and BG-subtracted. A residual BG usually remains that is due to laser-induced contamination (Raman, fluorescence) [12]. A second BG removal is usually performed using a Least-Square Fitting (LSF) of both BG parts located outside the Raman lineshape [13]. The experimental Raman spectrum is BG-subtracted thereupon in order to retrieve the Raman spectrum free from spurious contamination. Both the amplitude and integral of the lineshape may be used for quantitative analysis. We used lineshape integration as it provides a better counting statistics.

The Signal-to-Noise Ratio (SNR) is defined as:

$$SNR = \frac{S}{\sqrt{S+2\cdot B}} \quad (8)$$

where S is the Raman signal and B is the background, both integrated over a pixel range encompassing the lineshape [13].

Several companies (*e.g.* Kaiser, AXIOM, In-Photonics in the US, Horiba in France, to cite a few) already commercialize Raman immersion probes for monitoring pressures in the gas phase. These rod-shaped probes are convenient for process monitoring due to their low intrusiveness. A unique lens serves to focus the high-pass filtered laser light and to collect the Raman light, both signals being separated by a dichroic filter. The main drawback of this design is that the Raman light is often contaminated by Raman or fluorescence contributions from the optics as well as by residual laser light that must be heavily filtered out.

A free-space arrangement, with two orthogonally-placed fibers, in association with an Herriot-type multiple pass cell, was previously proposed by Spectral Sciences Co. (Burlington, MA, USA) and implemented by the NASA for the on-line hydrogen monitoring on a mobile launch platform [14]. They reported about a Limit of Detection (LOD) of about 100 ppm in a 15-s measurement time.

Recent developments implemented this design as well, *e.g.* Kiefer *et al.* [15] (Erlangen University, Germany), for monitoring input gases in combustion processes. They reported about a LOD for ethane of 1000 ppm for a 30-s integration time and 5-W laser power.

Finally, researchers of the Massachusetts Institute of Technology (MIT, Lexington, MA, USA) also performed free-space Raman measurements with a double-pass transverse arrangement, a high-throughput spectrometer (F/1.8) and large surface CCD [16]. They obtained LODs of the order of the ppm for an integration time of 15 s and a power of 10 W.

In the attempt of increasing the amount of collected Raman light, hollow waveguides were investigated as well by several authors [17-19]. The principle is to confine both laser and Raman lights over a distance much greater than the Rayleigh length (typically several tens of cm). An increase in Raman signal of about two orders of magnitude was reported with a 60-cm long silver-lined capillary by T.M. James *et al.* from Karlsruhe Institute of Technology (KIT, Germany) [17]. They announced a LOD of about 100 ppm for a laser power of about 1-2 W and measurement times of 10-100 s.

Using Photonics-Crystal Fibers (PCFs), hundred-fold factors were reported with hydrocarbon gas over traditional free-space configurations. Chow *et al.* [19] reported a LOD of 15 ppm for CO_2 with a 2.5-m long PCF (HC800-01, NKT Photonics, Denmark) and a laser power of 100 mW (@785 nm). In turn, significant delay times (several minutes) were reported in proportion with the device length due to diffusion kinetics of species inside the core. For instance, Chow *et al.* reported a filling time of about 10 minutes for a 2.5-m long PCF. Furthermore, PCFs are prone to contamination by aerosols whose size may be comparable to the core diameter (less than 10 micrometers).

For all these reasons, PCFs were not considered for Raman detection in this project and free-space Raman probes were designed instead.

B. Description of the Raman setup

The setup layout and Raman probe designed by the CEA are shown on Fig. 1a and Fig. 1b, respectively.

As a preliminary study, the probes designed for the project involve commercial off-the-shelf (COTS) components. Each probe is connected to the instrumentation by two separate pure silica-core (PSC), SMA-connected fibers, available from OFS Co. Unless otherwise indicated, the fiber used for transporting the laser light to the probe was a TCG-MA100H and that used to bring the Raman light back to the spectrometer was a TCG-MA200H. High-OH PSC fibers were chosen because of their improved radiation resistance at 640 nm compared to low-OH ones. A mounted lens (Thorlabs FiberPort PAF-SMA-5B) provides single-pass laser focusing and a beam dump eliminates the residual laser light.

In the context of H_2-risk management, there is no constraint on probe geometry or size. Therefore, we placed the collection fiber at the optimal distance *vs* laser beam and at 90° with respect to laser beam in order to improve the SNR in Raman detection.

A mobile rack incorporates a laser diode module (Modulight ML6540, @640 nm, 1 W, SMA905 output), an imaging spectrometer (ANDOR Shamrock 193i, 193-mm focus, F/3.6) equipped with a Si-based ultra-low noise Charge-Coupled Device (CCD iDUS416A-LDC-DD, 2000 x 256 pixels, ~ 0.01 e-/pix/s, cooled at -75°C), a laptop running the SOLIS software (ANDOR) and ancillary electronics. In this study, the equivalent readout noise is about 50 counts/min

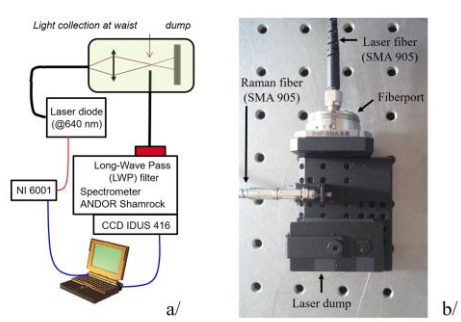

Fig. 1. Multitrack Raman setup used for the proof-of-concept of multi-gas Raman detection (a/), and top view of the probe (b/).

(over 50 vertical pixels). The quantum efficiency of silicon dramatically drops beyond 1000 nm (< 20 %) which imposes a laser wavelength less than 680 nm for H_2 detection.

The spectrometer accommodates four fiber inputs, each fiber mode imaged over successive rows (50 pixels each) onto the CCD surface (multitrack imaging). This design allows for simultaneous monitoring of Raman signals from four probes, providing cost-effective and simplified data analysis. In practice, the geometrical extent is limited by the aperture value of the spectrometer (F/#) and by the Rayleigh spectral criterion (chemical selectivity). In our case, # = 3.6 which gives a NA (= 1/2#) of only 0.14. Therefore, conventional fibers (NA = 0.22) are suitable and higher-NA fibers are not useful. A core diameter of 600 µm leads to the maximum allowed FWHM of 8 nm.

IV. Specifications for SA instrumentation

Design of PWRs include specifications for normal operation and for events for which they were not designed for (*i.e.* beyond design basis). The K_1 procedure of the French RCC-E standard (*Règles de Conception et de Construction, NF M 64-001*) was considered in this study. The K_1 conditions pertain to equipment located inside the containment of French PWRs subject to normal, seismic and accident conditions.

Table II lists the predicted environmental conditions for PWRs during an accident involving both fuel melting and damaged reactor vessel and concrete floor. Besides, probes installed inside the containment must comply with shock/vibration standards (Design Basis Earthquake - DBE) as any other electronuclear devices must do (DSD and SDD stand for *Demi-Séisme de Dimensionnement* and *Séisme De Dimensionnement* respectively). The probe should be housed within a lightproof protective stainless steel (SS) shell. Furthermore, the optical cables should be protected by SS cable ducts, providing partial radiological attenuation as well (*e.g.* by a factor of ½ at 1.25 MeV (^{60}Co)). Moreover, airborne particles (aerosols) may be released in the containment atmosphere. Previous RS experiments have been successfully performed in a steam jet seeded with particles of silicon carbide whose size is representative of fission products [7]. Finally, the instrumentation must remain operational during its entire lifetime (> 40 years) and withstand post-accidental conditions during at least several months.

In the following, we describe the metrological tests performed on custom-made Raman probes in compliance with RCC-E.

TABLE II
Environmental SA conditions for PWR

Parameter	Value	Observations
Relative humidity (%)	100	
Max. temperature (°C)	170	
Max. pressure (hPa)	9000	(9 bar)
Dose rate (ambient, ^{60}Co, kGy/h)	1	0.5 kGy/h under SS duct
Cumulated dose (ambient, MGy)	2	1 MGy under SS duct, within 6 months
Seismic (number of test)	5 / 1	DSD / SDD
Shock (J) / vibrations (g)	2 / 1	DBE

V. Qualifications of the Raman probe for gas monitoring in SA conditions

A. Calibration protocols in gas phase

A common approach is to evaluate relative pressures with respect to a reference specie of accurately known partial pressure, *e.g.* N_2. This "relative" procedure eliminates the need for temperature measurement and cancels out any fluctuation in laser power or collection efficiency. In turn, calibration laws *vs* pressure are nonlinear and this procedure might not be applicable to N_2-inerted containments (*e.g.* Boiling-Water Reactor - BWR). Furthermore, the pressure inside the containment must be known (available from control instrumentation of the NPP).

Another procedure is to evaluate absolute pressures of species, *i.e.* Eq. (9). This "absolute" procedure requires SA-qualified thermometers to measure the temperature within each Raman probe. Furthermore, it is necessary to insert a foreign material within the probe, partly illuminated by laser light. The additional Raman contribution from the material is then collected along with the Raman light from the gas and serves as intensity normalization. This "absolute" procedure provides linear calibration laws with respect to pressure and is applicable to N_2-inerted containments.

The following protocols were applied for the qualifications in gas phase, depending on species.

1) Climatic chamber (O_2, N_2, H_2O)

A climatic chamber (Voetsch VC2020), associated with a I-2000 thermo-hygrometer (Rotronics) were used at CEA LIST. During the test, the relative humidity (RH) was kept constant (80 %) and the temperature was adjusted in the range [10°C – 90°C]. The saturation water vapor pressures were estimated using the Antoine law:

$$Log_{10}\left(\frac{P_S}{P_{atm}}\right) = A - \frac{B}{T+C} \quad (9)$$

where P_s is the saturation pressure of water vapor and P_{atm} is the atmospheric pressure (typically ranging between 980 hPa and 1030 hPa), given by the nearby meteorological station. In the range [1°C – 99°C], the following values were considered: A = 8.07131, B = 1730.63, C = 233.426 °C.

The vapor pressure of water is then given by:

$$P(T) = P_s(T) \cdot RH \quad (10)$$

Natural atmosphere mainly contains O_2 (20.95 %), N_2 (78.08 %). The remaining (~ 1 %) is composed of trace gases such as methane (CH_4), argon (Ar) and carbon dioxide (CO_2). Partial pressures for O_2 and N_2 are then estimated as follows:

$$P_{N2} = 0.7808 \cdot (0.9903 \cdot P_{atm} - P_{H2O}) \quad (11)$$

$$P_{O2} = 0.2095 \cdot (0.9903 \cdot P_{atm} - P_{H2O}) \quad (12)$$

Fig. 2 shows the evolution of the Raman spectra of O_2, N_2 and H_2O as the temperature rises.

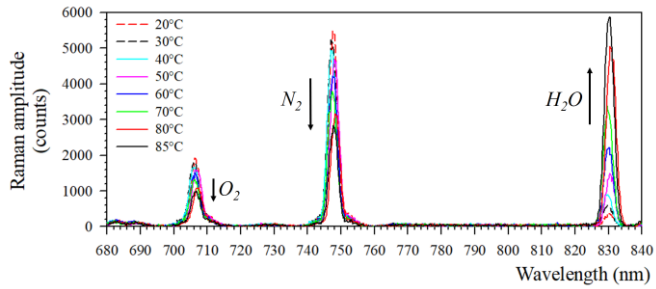

Fig. 2. Evolution of the Raman spectra of O_2, N_2 and H_2O as the temperature rises (integration time = 200 s, atmospheric pressure).

Fig. 3 shows the evolution of the Raman signal (multiplied by the temperature in K) with respect to partial pressures in the gas phase, calculated from Eq. (11)-(12). The data follow a linear trend, as expected from Eq. (5), without hysteresis. The integration time was 200 s and laser power was 0.7 W.

Fig. 4 shows the evolution of the normalized Raman signals of O_2 and H_2O with respect to that of N_2. One can see that the relative Raman signal of O_2 is constant *vs* N_2, as expected because the air mixture did not change during the experiment.

The calibration curve of the Raman signal of water vapor is nonlinear because the partial pressure of N_2 actually decreases inversely with that of water vapor. Taking into account the uncertainty associated with Raman measurements, the LODs were estimated to be about 9 hPa for H_2O, 16 hPa for O_2 and 22 hPa for N_2 in this experimental configuration.

2) *Flame propagation tube (N_2, H_2)*

The SSEXHY installation (*Structure Soumise à des Explosions d'HYdrogène*) of the CEA-Saclay (DEN/DM2S) is a flame propagation tube with closed extremities. Flame accelerations of premixed H_2-air mixtures are obtained at many combustion regimes by adjusting inner blocking plates.

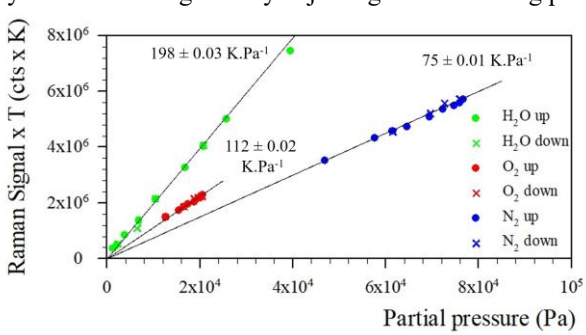

Fig. 3. Calibration relation of O_2, N_2 and H_2O with respect to partial pressure in the gas phase ("absolute" mode).

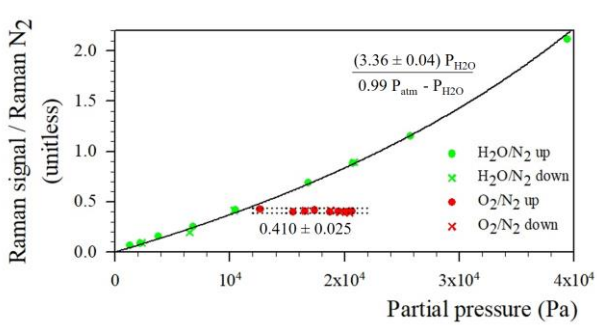

Fig. 4. Calibration relation of O_2 and H_2O with respect to partial pressure in the gas phase ("relative" mode, *vs* nitrogen).

This installation was used for both calibrating the Raman signal *vs* H_2 pressure and performing combustion tests as the probe was blocked inside the tube. The air was vacuum-pumped out of the tube, prior to gas injection with a calibration gas cylinder (5 % H_2, 95 % N_2), in order to avoid stratification. The gas pressure was adjusted with the help of a manual flow controller and manometer until the expected pressure was reached in the range of 0 – 100 % of atmospheric pressure (H_2 pressure was thus adjusted from 0 to 500 hPa).

A dedicated feedthrough was adapted onto the tube. For this experiment (Fig. 5), a 600-µm diameter fiber (HCP 600) was used for collecting the Raman light, the laser power was 0.7 W and the temperature was kept constant (22°C). The experimental BG-subtracted Raman lineshapes are shown in Fig. 6. Both vibronic and rotational modes of H_2 are visible as well as the vibronic mode of N_2. The Raman signal is linear with H_2 pressure and the LOD is about 0.35 hPa (360 s) and 2.3 hPa (60 s). Finally, we performed a combustion test using a mixture of 11 % H_2 and 89 % air. The probe did not suffer any damage because of the low dissipated thermal energy.

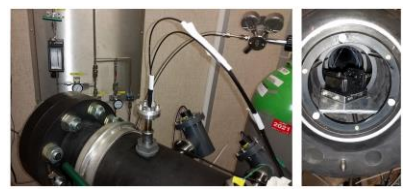

Fig. 5. View of the calibration experiment with the flame propagation tube (left), probe blocked inside the tube (right).

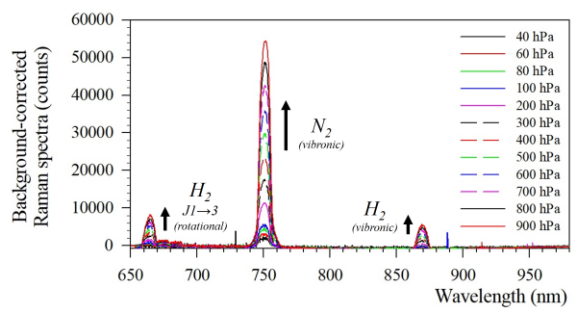

Fig. 6. Experimental Raman spectra recorded for several pressure inside the tube (all spectra are BG-corrected, integration time = 6 minutes).

B. *Irradiation test*

We conducted an irradiation test in the Poseidon irradiation cell (CEA Saclay) with the aim to check the behavior of the Raman probe under radiation and to estimate the amount of Radiation-Induced Attenuation (RIA) and Cerenkov light generated within the fibers. The Poseidon cell consists in two source walls (^{60}Co, 1.25 MeV, 300 kCi) encompassing the device under test and providing a planar isodose surface of 0.5 m^2. The near-contact dose rate was ~ 5.8 kGy/h and the maximum dose was 1.92 MGy (331 hours). The probe was inserted into a box, heated up at 80°C. The exposed Raman fiber was 5-m long. A second fiber (TCG-MA100H) was deployed back and forth inside the cell in order to measure the RIA (in transmission). We alternatively performed RIA and Raman/Cerenkov measurements with the same spectrometer.

Fig. 7 shows the RIA with respect to time. As a rule-of-thumb, the RIA changes with the square root of the dose with high-OH PSC fibers. The RIA at 640 nm was not measured

due to the presence of the cutoff filter but it was estimated to be about 2.5 dB/m for a dose of 1 MGy (see Table II).

In practice, the influence of RIA is compensated for by an increase in integration time. The maximum allowed RIA is estimated to be about 10 dB so that the fiber length cannot exceed 4 meters. Furthermore, the probe remained functional after the irradiation test, although epoxy connectors failed, as expected. A 20 %-drop in Raman efficiency is found (-1 dB).

The second important result is the recording of Cerenkov light that actually superimposes over the useful Raman signal. A Cerenkov effect occurs when charged particles (essentially electrons) travel faster than the speed of light in the material (relativistic effect). For silica (refractive index ~ 1.46), the energy threshold is 180 keV. The power spectral density (PSD) of the continuum Cerenkov spectrum evolves as the inverse third power of wavelength.

B. Brichard *et al.* attempted to use this effect for the in-core monitoring of reactor power [20]. For a 200-µm fiber, they reported about a PSD of -72 dBm (spectral width = 10 nm), *i.e;* 6 fW/nm at 870 nm for 1-m long fiber, under a 2 kGy/s dose rate (7.2 MGy/h). Transcribed into homogeneous units, the PSD is then ~ 0.8 $fW.nm^{-1}/(kGy//h)$, per meter of fiber.

At 870 nm, we recorded a PSD of 21 fW/nm for a 5-m long exposed fiber. The PSD is then about 0.78 $fW.nm^{-1}/(kGy/h)$ per meter of fibre, in accordance with [20]. Transposed into K_1 conditions (500 Gy/h, under cable duct), the PSD of the Cerenkov light is 580 times greater than that of Raman of N_2 (0.78 atm = 780 hPa), calling for alleviating measures.

The first measure consists in arranging a synchronous detection with laser emission as the Raman signal is correlated with it. By doing so, the SNR increases with the square root of scan number, enabling the recovery of the useful signal even when overwhelmed within a stronger Cerenkov contribution.

We performed another experiment with a 6-MV Varian Linatron LINAC (average energy ~ 1.5 MeV) at lower dose rates with the aim to test the on-line averaging algorithm. Both Raman probe and its 5-m long collection fiber were exposed to the photon beam. The fiber was spun perpendicularly to the beam axis, as in Poseidon. Fig. 8 shows the Raman spectra of air mixed with the Cerenkov contribution for several dose rates. Without Cerenkov, the SNR for the N_2-peak (780 hPa) is about 171 for an integration time of 5 minutes (*i.e.* 5 scans of 60 s each). In presence of Cerenkov light, the SNR drops down to about 33, 28.5 and 25 for 14 Gy/h, 23 Gy/h and 30 Gy/h respectively. For instance, the integrals of both the N_2 Raman lineshape and Cerenkov contribution over a range of ±4 nm yields about 8850 cts and 314 10^3 cts respectively. Taking into account 5 scans (√5 ~ 2.23), the SNR for the N_2

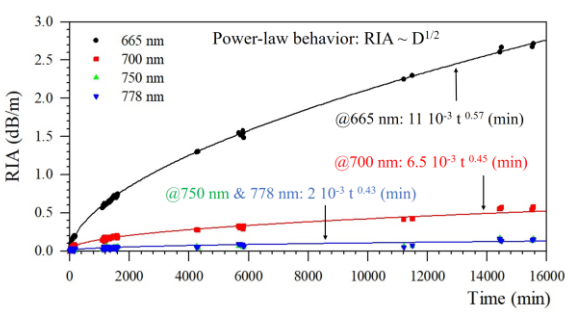

Fig. 7. Experimental RIA recorded with the High-OH fiber during the Poseidon experiment, at several wavelengths (dose rate = 5.8 kGy/h).

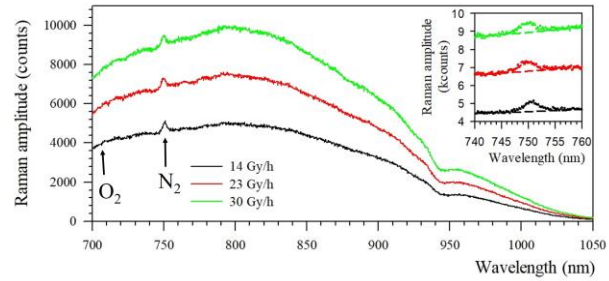

Fig. 8. Raman spectra recorded with the Raman probe with an exposed fiber length of 5 meters (6-MV LINAC photon beam) for several dose rates (14 Gy/h, 23 Gy/h, 30 Gy/h). Data are averaged over 5 scans of 60 s each. Inset shows the Raman peak of N_2 and the baseline used for SNR estimation.

detection (Eq. (8)) is about 25 for a dose rate of 30 Gy/h and 5-min integration time. Transposed to the detection of H_2 (Cf. Table I), a H_2 pressure of 10 hPa is detectable (SNR = 1) within 5 minutes, with an exposed fiber length of 5 m and a dose rate of 14 Gy/h. However, the time required to achieve this for a dose rate of 500 Gy/h (see Table II) is typically of several hours, still too long concerning SAMG.

C. Metrological validation of the Raman probes in representative thermodynamic conditions

Thermo-hydraulic tests were conducted in the MISTRA facility (CEA Saclay), representative of a PWR containment at a 1/10 linear length scale [21] (Fig. 9). Four Raman probes were inserted within the containment, fiber-coupled to the instrumentation through eight optical penetrations. Sampled Mass Spectrometry (SMS) monitored gas pressures during the course of the experiment and both pressure and temperatures were recorded as well. O_2, N_2, H_2O were injected at elevated temperature (160°C) and high pressure (4 10^5 Pa (4 bar)). The maximum probe temperature was 130°C. At this time, the probes were not Joule-heated so that condensation prevented Raman measurements during the first hour of experiment prior to thermal equilibrium between probes and vapor.

The concentration in water vapor was estimated from the Raman signal of H_2O relative to that of N_2. Both Raman and SMS measurements are in accordance; a relative deviation of ± 2 % is attributed to gas heterogeneities.

D. Shock/vibration and steam jet tests

Shock and vibration tests were performed at the *Laboratoire National d'Essais* (LNE, Nimes, France), according to electronuclear standards (EN-60028-6-75 and EN-60028-2-6 respectively). The probe was mounted with silicone inside a SS protective package and fixed onto a 3-axis shaking table equipped with accelerometers for 3-axis vibration tests (frequency range = [10 Hz – 500 Hz]). We performed an endurance test (20 cycles, 1 g) followed by a frequency scan at

Fig. 9. View of the MISTRA facility (CEA Saclay) [21] (left) and installation of the probes inside the containment (right)]

0.2 g in order to evaluate natural frequencies and to check for potential degradations. The cutoff frequency of the silicone-case assembly was too high (~ 300 Hz) and ineffective. Then, a freefall impactor (480 g, 40 cm) provided 2-J energy shocks. The probe survived both tests.

Finally, the probe was equipped with constantan (Cu-Ni, 30 Ω/m) wires in order to provide Joule heating of the optics parts (objective and extremity of collection fiber) so as to prevent water condensation. Both wires (resistance ~ 8 Ω) were coated by a Teflon tube and connected to a power supply (8 V, 6 A) providing a contact temperature of 90 °C. We inserted two high-pass filters (Thorlabs FES0650) into the optical circuit in order to filter out the upper contribution of the laser spectrum. With this setup, it was possible to record Raman spectra of ambient air within a vertical steam jet.

VI. Conclusions

Raman spectrometry is an interesting alternative for H_2-risk assessment within NPP's containment during a severe accident because it is a simple, compact, flexible and chemical-selective technique (no interference between species) that involves only one laser and spectrometer equipped with a Si-based 2D CDD. Free-space, single-pass transverse probes are compact, robust (passive optics, no electronics), and may be radiation-hardened. The associated readout unit, placed away from the radiological perimeter, is fiber-connected to the probes located inside the containment and potentially powered by emergency power supplies in case of power outage.

Custom-made fiber-coupled Raman probes were qualified in a climatic chamber, a flame-propagation tube, a ^{60}Co irradiation cell, a 3D shaking table, a steam jet and the MISTRA facility (1/10-scale thermo-hydraulic containment of the CEA). Additional SA-qualified sensors are yet necessary to provide pressure and temperature measurements. The laser wavelength of 640 nm was chosen in order to efficiently detect the Raman contribution from H_2 (870 nm). Typical LODs of about 10 hPa are obtained for all species of interest (O_2, N_2, H_2O, H_2, CO_2), with PSC fibers (Ø = 200 µm, NA = 0.22), for integration times of several minutes.

All qualifications successfully passed except the irradiation test. First, the RIA (1 MGy, 5 meters) is still too high (2.5 dB/m at 640 nm), limiting the fiber length to about 4 meters, and pushing towards the use of higher laser wavelengths (up to 680 nm with a Si-based CCD). Second, Raman detection is spoiled by Cerenkov light that is 580 times greater than the Raman signal of N_2 (780 hPa, 500 Gy/h), necessitating alleviating measures. A synchronous detection provides an improvement in SNR: LINAC experiments have shown that a pressure of 10 hPa (1 %) of H_2 is detectable within 5 minutes for a dose rate of 14 Gy/h. Other solutions are necessary in order to comply with K_1 conditions. First, multiple-pass or optical confinement techniques will increase the Raman efficiency of the probe. Second, the use of PCFs in replacement to PSCs would reduce the amount of Cerenkov [22] as light mostly propagates in air rather than in silica. A more efficient probe design is currently under investigation. It will incorporate heating wires and a mechanical design preventing optics contamination by aerosols.

References

[1] A. Bentaïb, N. Meynet and A. Bleyer, "Overview on hydrogen risk research and development activities: methodology and open issues," *Nucl. Eng. Technol.*, vol. 47, pp. 26-32, 2005

[2] Z.M. Shapiro and T. R. Moffette, "Hydrogen flammability data and application to PWR Loss-Of-Coolant Accident," *WAPD--SC-545*, 4327402, Pittsburgh, PA, 1957

[3] A. Omoto, "The accident at TEPCO's Fukushima-Daiichi Nuclear Power Station: What went wrong and what lessons are universal ?," *Nucl. Instr. Methods*, A, vol. 731, pp. 3-7, 2013

[4] A. Hill, "Multi-functional containment atmosphere monitoring," NUSSA Workshop, Sept 7-8, 2012, Beijing, China

[5] T. Hübert, L. Boon-Brett, G. Black and U. Banach, "Hydrogen sensors – a review," *Sens. Actuators*, B, vol. 157, pp. 329-352, 2011

[6] A. Campargues, S. Kassi, K. Pachucki and J. Komosa, "The absorption spectrum of H_2:CRDS measurements of the (2-0) band, review of the literature data and accurate *ab initio* line list up to 35 000 cm^{-1}," *Phys. Chem. Chem. Phys.*, vol. 14, pp. 802-815, 2012

[7] E. Porcheron, L. Thause, J. Malet, P. Cornet, P. Brun, J. Vendel, "Simultaneous application of Spontaneous Raman Scattering and LDV / PIV for steam / air flow characterization," 10th International Symposium on Flow Visualization (ISFV-11), Kyoto, 2002.

[8] H.W. Schrötter and H.W. Klöckner, Ch. 4, "Raman scattering cross sections in gases and liquids," pp. 123-164, in "Raman Spectroscopy of gases and liquids," Ed. By A. Weber, Topics in Current Physics, Springer-Verlag, 1979

[9] W.F. Murphy, W. Holzer and H.J. Bernstein, "Gas-phase Raman intensities: A review of "pre-laser" data," *Appl. Spectrosc*., vol. 23, n°3, pp. 211-218, 1969

[10] D.G. Fouche and R.K. Chang, "Relative Raman cross-section for O_3, CH_4, C_3H_8, NO, N_2O and H_2," *Appl. Phys. Lett.*, vol. 20, n°7, 1972, pp. 256-257

[11] W.R. Fenner, H.A.Hyatt, J.M. Kellam and S.P.S Porto, "Raman cross section of some simple gases," *J. Opt. Soc. Am.*, vol. 63, n°1, pp. 73-77, 1973

[12] I. Latka, Latka, S. Dochow, C. Krafft, B. Dietzek and J. Popp, "Fiber optics probes for linear and nonlinear Raman applications – Currents trends and future developments," *Laser Photonics Rev.*, vol.7, n°5, pp. 698-731, 2013.

[13] M. Schlösser, "Accurate calibration of Raman systems," Doctoral Thesis, Springer, 2014 (ISBN 978-3-319-06221-1)

[14] S.M. Adler-Golden, N. Goldstein, F. Bien, M.W. Matthew, M.E. Gersh, W.K. Cheng and F.W. Adams, "Laser Raman sensor for measurement of trace-hydrogen gas," *Appl. Opt.*, vol. 31, n°6, pp. 831-835, 1992

[15] J. Kiefer, T. Seeger, S. Steuer, S. Schorsch, M.C. Weikl and A. Leipertz, "Design and characterization of a Raman-scattering-based sensor system for temporally resolved gas analysis and its application in a gas turbine power plant," *Meas. Sci. Tech.*, vol. 19, 085408, 2008

[16] R.L. Aggarwal, L.W. Farrar, S. Di Cecca, M. Amin, B.G. Perkins, M.L. Clark, T.H. Jeys, D.W. Sickenberger, F.M. D'Amico, E.D. Emmons, S.D. Christensen, R.J. Kreis and G.K. Kilper, "Chemical aerosol Raman detector," *Rev. Sci. Instrum.*, vol. 88, 033107, 2017

[17] T.M. James, S. Rupp, H. H. Telle, "Trace gas and dynamic process monitoring by Raman spectroscopy in metal-coated hollow glass fibres," *Anal. Methods*, vol. 7, pp. 2568-2576, 2015

[18] M.P. Buric, K.P. Chen, J. Falk and S.D. Woodruff, "Enhanced spontaneous Raman scattering and gas composition analysis using a photonic crystal fiber," *Appl. Opt.*, vol. 47, n°23, pp. 4255-4261, 2008

[19] K.K. Chow, M. Short, S. Lam, A. McWilliams, H. Zeng, "A Raman cell based on hollow-core photonic crystal fiber for human breath analysis," *Med. Phys.*, vol. 41, n°9, pp. 092701-1/9, 2014

[20] B. Brichard, A.F. Fernandez, H. Ooms, F. Berghmans, "Fibre-optic gamma-flux monitoring in a fission reactor by means of Cerenkov radiation," *Meas. Sci. Technol.*, vol. 18, pp. 3257-3262, 2007

[21] E. Studer, J.P. Magnaud, F. Dabben and I. Tkatschenko, "International standard problem on containment thermal-hydraulics ISP47 – Results from the MISTRA exercise," *Nucl. Eng. Des*., vol. 237, pp. 536-551, 2007

[22] S. Girard, J. Baggio and J-L. Leray, "Radiation-Induced effects in a new class of optical waveguides: the air-guiding Photonic Crystal Fibers," *IEEE Trans. Nucl. Sci.*, vol 52, n°6, pp. 2683-2688, 2005